

Concentration Trajectory Route of Air pollution with an Integrated Lagrangian Model (C-TRAIL Model v1.0) Derived from Community Multiscale Air Quality Model (CMAQ Model v5.2)

1 Arman Pouyaei ¹, Yunsoo Choi ¹, Jia Jung ¹, Bavand Sadeghi ¹, Chul Han Song²

2 ¹ Department of Earth and Atmospheric Sciences, University of Houston, Houston, TX, USA

3 ² School of Environmental Science and Engineering, Gwangju Institute of Science and Technology (GIST), Gwangju, South
4 Korea

5 *Correspondence to:* Yunsoo Choi (ychoi6@uh.edu)

6 **Abstract.** This paper introduces a reliable and comprehensive Lagrangian output (Concentration Trajectory Route of Air
7 pollution with an Integrated Lagrangian model, C-TRAIL version 1.0) from a Eulerian air quality model for validating the
8 source-receptor direct link by following polluted air masses. To investigate the concentrations and trajectories of air masses
9 simultaneously, we implement the trajectory-grid (TG) Lagrangian advection scheme in the CMAQ (Community Multiscale
10 Air Quality) Eulerian model version 5.2. The TG algorithm follows the concentrations of representative air "packets" of species
11 along trajectories determined by the wind field. The diagnostic output from C-TRAIL accurately identifies the origins of
12 pollutants. For validation, we analyze the results of C-TRAIL during the KORUS-AQ campaign over South Korea. Initially,
13 we implement C-TRAIL in a simulation of CO concentrations with an emphasis on the long- and short-range transport effect.
14 The output from C-TRAIL reveals that local trajectories were responsible for CO concentrations over Seoul during the stagnant
15 period (May 17-22, 2016) and during the extreme pollution period (May 25-28, 2016), highly polluted air masses from China
16 were distinguished as sources of CO transported to the Seoul Metropolitan Area (SMA). We conclude that during this period,
17 long-range transport played a crucial role in high CO concentrations over the receptor area. Furthermore, for May 2016, we
18 find that the potential sources of CO over that SMA were the result of either local transport or long-range transport from the
19 Shandong Peninsula and, in some cases, from north of the SMA. By identifying the trajectories of CO concentrations, one can
20 use the results from C-TRAIL to directly link strong potential sources of pollutants to a receptor in specific regions during
21 various time frames.

22

23 **Keywords:** C-TRAIL, Trajectory analysis, CMAQ, East Asia, KORUS-AQ campaign

24 **1 Introduction**

25 Determining the long-range transport (LRT) of pollutants has been a challenge for air quality researchers. As the chemical
26 composition of outflow over a region or continent can significantly affect air quality downwind, information about LRT must
27 be reliable. Several studies have applied a number of methods to examine the role that LRT plays in the concentrations of
28 particulate matter (PM), ozone, trace gases, and biomass burning tracers over target regions (Stohl, 2002). For instance, several
29 sources (Choi et al., 2014; Lee et al., 2019; Oh et al., 2015; Pu et al., 2015) have applied the NOAA Hybrid Single-Particle
30 Lagrangian Integrated Trajectory (HYSPLIT) model (Draxler, 1998) and back-trajectory analyses in an attempt to identify
31 possible sources of PM in East Asia. The HYSPLIT model is a widely used tool that has been incorporated into other chemical-
32 transport models (CTMs) to measure the LRT of ozone, carbon monoxide (CO), and aerosols to establish the source-receptor
33 relationship of air masses over the United States (Bertschi and Jaffe, 2005; Carroll et al., 2008; Gratz et al., 2015; Price et al.,
34 2004; Sadeghi et al., 2020; Weiss-Penzias et al., 2004). Several studies have used another model, the FLEXTRA trajectory
35 model (Stohl, 1996; Stohl and Seibert, 1998), to capture the background source regions of high-PM over East Asia and quantify
36 the contributions from these regions (Lee et al., 2011, 2013). Furthermore, this model also has been applied to some European
37 regions to explain the potential advected contribution of aerosols (Cristofanelli et al., 2007; Petetin et al., 2014; Salvador et
38 al., 2008). Several studies have recently attempted to develop new trajectory models that overcome truncation errors that
39 originate from schemes for numerically integrating trajectory equations (Döös et al., 2017; Rößler et al., 2018) and to link
40 trajectories to specific trace species (Kruse et al., 2018; Stenke et al., 2009). Another widely used tool for studying the
41 distribution of CO, ozone, PM, and other aerosols for both air quality forecasting and emission scenario analysis is the EPA
42 Community Multiscale Air Quality (CMAQ) model (Byun and Schere, 2006). CMAQ, with the help of meteorological inputs
43 from the Weather Research and Forecasting (WRF) model, or advanced machine learning-based methods (Eslami et al., 2019;
44 Lops et al., 2019; Sayeed et al., 2020), assists policy-makers with solving pollution-related issues by legislating regulations.
45 Spatial concentration patterns of pollutants incorporated with other models (i.e., back-trajectory models) or satellite data
46 enhance our understanding of the impact of LRT and other related processes such as the formation of aerosols, emissions, and
47 dry deposition in various regions (Chen et al., 2014; Chuang et al., 2008, 2018; Souri et al., 2016; Wang et al., 2010; Xu et al.,
48 2019; Zhang et al., 2019).

49
50 The conventional way of estimating potential source regions of air-mass transport is to use back-trajectory modeling.
51 Frequently used for source-receptor linkage, such models combine their output with measurements of pollutant concentrations.
52 As this source-receptor linkage approach uses meteorology-based models for back trajectories, it is not fully accepted because
53 it is unable to directly determine whether an originated air mass is polluted or non-polluted (Lee et al., 2019). Thus, back-
54 trajectory modeling provides unreliable information from which to assess the variation of pollutants at a receptor point, raising
55 concern about its use for interpreting the contribution of the effect of LRT on concentrations of a target pollutant. In addition,
56 other factors such as emissions and the local production of air pollutants contribute to variation in a target pollutant. Although

57 aircraft campaigns in several regions have applied a Lagrangian approach to interpreting variations in concentrations, they
58 have not effectively addressed the above concern. After all, such campaigns are neither frequent nor continuous.

59
60 In this study, we implement a Lagrangian advection scheme that we refer to as the trajectory grid (TG) (Chock et al., 1996),
61 into the Eulerian CMAQ v5.2 model. We introduce a new type of output from the concentration trajectory route of air pollution
62 with the integrated Lagrangian (C-TRAIL v1.0) stand-alone model in addition to CMAQ v5.2 output to simultaneously
63 accomplish two objectives: (1) to provide a direct link between polluted air masses from sources and a receptor and (2) to
64 provide the spatial concentration distribution of several pollutants to explain relevant physical processes. Chock et al. (2005)
65 incorporated the TG into an air quality model to study the accuracy of this Lagrangian advection method over the Bott
66 advection scheme applied in the Eulerian domain. One significant outcome of the TG model applied to CTMs is its ability to
67 account for the concentrations of pollutants in air masses in its investigation of trajectories, which addresses the unreliability
68 of meteorology-based Lagrangian models when the pollutedness or cleanliness of an originated air mass becomes an issue.
69 For this study, we have selected CO. As this pollutant has an oxidation lifetime of approximately two months, it is an ideal tracer
70 with which we can study its impact on LRT without having stable background levels such as CO₂ (Heald et al., 2003; Liu et
71 al., 2010; Vay et al., 2011). Furthermore, as CO is produced mainly by the incomplete combustion of carbon-containing fuels
72 (Halliday et al., 2019), it is an ideal proxy with which we can relate concentrations of receptors to sources of traffic or power-
73 plant emissions. We begin by introducing the methodology behind TG and the implementation of TG into CMAQ. Then, we
74 present a simple case and our interpretation of the C-TRAIL output. Finally, we present a case study of C-TRAIL for Korea
75 and the United States Air Quality (KORUS-AQ) campaign over South Korea.

76 **2 Methodology**

77 **2.1 Description of the TG approach**

78 To solve the transport equation, Chock et al. (1996) presented the TG approach in air quality modeling. This approach, which
79 entails transporting points on a concentration profile along their trajectories in a Lagrangian manner, uses the Eulerian approach
80 for diffusive transport. From now on, we will refer to these points as “air packets” for two reasons: (1) Their nature is similar
81 to that of air parcels, but they are much smaller, and (2) they behave much like particles, but they carry information about
82 several species. The TG method rewrites the advection equation for concentration as follows:

$$83 \quad \frac{dc}{dt} = \frac{\partial c}{\partial t} + \mathbf{v} \cdot \nabla c = -(\nabla \cdot \mathbf{v})c, \quad (1)$$

84
85 where c is the concentration of species in a velocity field \mathbf{v} . The Lagrangian approach divides the total derivative of the
86 concentration into a full derivative of concentration with respect to time, $\frac{dc}{dt}$, and a remaining term containing velocity

87 divergence, $-(\nabla \cdot \mathbf{v})C$. Following this approach, the TG automatically and accurately conserves the mass, sign, and shape of
88 the concentration profile. As interpreted from the equation, the concentration profile of the species along trajectories can be
89 described. Otherwise stated, after determining the location of a packet and the concentration inside the domain, we are able to
90 assess the concentration profile along its trajectory. Since all species represented in one packet and all of the packets move in
91 the flow field according to the wind velocity, differentiating between advection equations for each species (as is done in
92 Eulerian advection schemes) is no longer necessary; thus this removes the associated numerical errors with the discretization
93 of the advection equation. The concentration of each packet along its trajectory can be determined by the following equation:
94

$$C(t) = C(t_0) \exp\left(-\int_{t_0}^t (\nabla \cdot \mathbf{v}) dt\right) \approx C(t_0) \exp[-(\nabla \cdot \mathbf{v})(t - t_0)], \quad (2)$$

95 where $C(t)$ is the concentration of species at the location of a packet as it moves along its trajectory. Since we can use the TG
96 method to calculate the concentration from an ordinary differential equation, it is mass conserving, monotonic, and accurate.
97 In the diffusion step, however, interpolation errors occur, but they are typically considerably smaller than Eulerian advection
98 errors (Chock et al., 2005). In addition, the trajectory will be three-dimensional and as accurate as of the input for wind velocity
100 and direction. In particular, for large-scale vertical winds, in which CTMs typically modify the scheme to address the mass-
101 conservation issue, TG will remove numerical diffusion from upwind vertical advection schemes and generate more physical
102 vertical winds (Hu and Talat Odman, 2008). It is noteworthy to mention that units for the concentration of species are referred
103 to as “ppbv” or “ μgm^{-3} ” depending on the species type, and the unit conversion is taken into account in the process of solving
104 equations.

105 **2.2 Implementation of TG in CMAQ v5.2**

106 In this section, we briefly describe the key features of TG implementation in the CMAQ v5.2 model, a Eulerian model
107 consisting of several modules (i.e., advection, diffusion, cloud, and aqueous-phase). The C-TRAIL v1.0 model utilizes the
108 same meteorology, initial conditions (ICs), boundary conditions (BCs), and emissions that CMAQ requires. All of the CMAQ
109 modules and parameters are associated with cells of the Eulerian grid on the model domain. Since TG is based on CMAQ in
110 this study and some of the CMAQ processes cannot be satisfactorily carried out by Lagrangian models (e.g., eddy diffusion)
111 at this time, grid cells are the primary structure for initiating and listing packets. By grouping the packets into grid cells,
112 keeping track of which packets are close to each other is easier. While the grid cells of Eulerian models represent Eulerian-
113 type outputs, tracking the packets of Lagrangian advection provides both their trajectories and their concentrations (Figure 1).

114
115 The process of advection for packets follows the ordinary differential equation:

$$\frac{dy(t)}{dt} = \mathbf{V}(\mathbf{y}(t), t), \quad (3)$$

116 where \mathbf{V} [ms⁻¹] is the three-dimensional wind velocity and $\mathbf{y}(t)$ [m] is the position vector of packets at time t [s]. The equation
117 is solved using the following simple predictor-corrector scheme:

$$\mathbf{y}^i(t + \Delta t) = \mathbf{y}(t) + \mathbf{V}(\mathbf{y}(t), t)\Delta t \quad (4)$$

$$\mathbf{y}^f(t + \Delta t) = \mathbf{y}(t) + 0.5[\mathbf{V}(\mathbf{y}(t), t) + \mathbf{V}(\mathbf{y}^i(t + \Delta t), t + \Delta t)]\Delta t, \quad (5)$$

118 where \mathbf{y}^i is the initial estimate of the new position from the predictor step and \mathbf{y}^f is the final position calculated by the
119 corrector step. When the initiated packets in the domain follow the Lagrangian equation, they land in different grid cells after
120 each time step. To balance the density of packets in grid cells, we apply a simple packet management technique that includes
121 spawning (filling) and pruning (emptying) processes. In the spawning process, every step entails the creation of a group of
122 new packets in each cell with too few packets. The initial composition of a spawned packet is estimated from nearby packets.
123 The pruning process entails the removal of extra packets from cells that have become overpopulated. During this process, the
124 packets closest to the cell center are retained. Such packet management with favorable options contributes to reducing the
125 computational costs of the C-TRAIL model. The limitation of this packet management approach, however, is that it incurs
126 mass conservation by adding minor interpolation errors. The underlying algorithms for both vertical and horizontal diffusion,
127 emissions, and other processes are the same as those in standard CMAQ (Byun and Schere, 2006) with some minor
128 modifications. The coupling of Eulerian diffusion and TG advection at each time step is accomplished by first taking the
129 average of concentrations from all packets in each cell as cell average. Then, by considering each packet as a cell and cell
130 average representative of the neighboring cells, we use a predictor-corrector method for determining the concentration of each
131 packet. Figure 2 summarizes the process of C-TRAIL from initialization to output generation. By combining the locations of
132 the packets in each time step during the 24 hours, we generate the 24-hour trajectory of each packet.

133 3 Setup and Validation of the Model

134 In this study, we implement TG in the CMAQ model version 5.2. Shown in Figure 3, the model domain, with a horizontal grid
135 resolution of 27-km over East Asia, covers the eastern parts of China, the Korean Peninsula, and Japan. We use the 2010 MIX
136 emission inventory (Li et al., 2017) at a 0.25-degree spatial resolution. The emission inventory contains monthly averaged
137 carbon bond version 5 (Sarwar et al., 2012) emission information, which includes ten chemical species, including CO, in five
138 different sectors. We also use the 2011 Clean Air Policy Support System emission high-resolution (1-km) inventory from the
139 National Institute of Environmental Research for Korea, which contains the area, and the line and point sources of a variety of
140 species, including CO. We provide WRF model v3.8 output as meteorological inputs in our CMAQ model. We validate our
141 WRF model's wind predictions with surface measurements and radiosonde measurements for the KORUS-AQ period (see
142 Table S1-S2 and Figure S1-S4). Jung et al. (2019) validated the air quality model set up in a comparison between aerosol
143 optical depths from simulations and observations; they showed a correlation of 0.64 for the entire KORUS-AQ campaign
144 period. Their comparison of various gaseous and particulate species also showed close agreement with observations.

146 We run C-TRAIL simulations for May 2016 during the KORUS-AQ campaign. In papers pertaining to this campaign, several
147 studies (Al-Saadi et al., 2016; Choi et al., 2019; Miyazaki et al., 2019) have separated the time frame into three periods (Table
148 1) based on meteorological conditions: 1) the dynamic weather period (DWP), a rapid cycle of clear and rainy days in the
149 Korean Peninsula (May 10-16); 2) the stagnant period (SP), in which the area was under the influence of a high-pressure
150 system (May 17-22) and which showed the influence of local emissions; and 3) the extreme pollution period (EPP) with high
151 peaks of pollutants that showed strong direct transport from China (May 25-28).

152

153 The overall accuracy of the CMAQ CO simulation compared to that of aircraft measurements during all periods is presented
154 in Figure 4(a). The correlation between the modeled CO concentrations and the observations at different altitudes for all of
155 May 2016 was 0.71, indicating that the performance of the model is sufficiently reliable for a study of the source of CO
156 concentration (Table 1). Figure 4 shows the under-prediction of the model during the DWP and SP. The model, however,
157 showed a very high correlation during the EPP compared to higher CO observations over the Korean Peninsula. We also
158 provided CMAQ's CO comparison with surface station measurements in the supplementary document (see Table S3 and
159 Figure S5). The results of this comparison also show the model's underprediction, which is caused by uncertain emission
160 inventories over East Asia. The C-TRAIL outputs of the mentioned periods will be discussed in Section 3.3.

161

162 The Eulerian output from CMAQ, including CO concentrations and surface wind fields, is displayed in Figure 5. High peaks
163 of CO concentrations appeared in southeastern China, including the Shanghai region and the Shandong Peninsula, because of
164 high anthropogenic emissions in these areas. The impact on pollution from LRT was greater in this region because the dominant
165 wind over East Asia in May was westerly, which explains why high concentrations of CO were observed over the Yellow Sea.
166 Also observed over the Yellow Sea during this period was a shallow anticyclone (a common phenomenon in this region that
167 affects the regional transport of pollution). From a thorough investigation of CO concentrations and wind patterns during
168 various meteorological periods, we provide the following major findings: 1) During the DWP, a mixed response from the LRT
169 of CO and local emissions occurred. Also, in light of the impact of convection, the concentrations of CO over Korea could
170 have increased or decreased by vertical wind transport and cloud updrafts and downdrafts. Owing to the dynamic nature of
171 this period (i.e., cloudy, rainy, or clear), the interpretation of the LRT effect by conventional methods posed a challenge. 2)
172 During the SP, a high-pressure system settled over the Korean Peninsula, which explains the extremely low wind speed and
173 the stagnant air, the latter of which eliminated the impact of LRT. Even though one might assume that the model would produce
174 more accurate simulations with less convection-related transport, CO concentrations were significantly underestimated by the
175 model (Jeon et al., 2016) because of uncertainties in the chemistry modeling and the faulty emission inventories over East
176 Asia. 3) During EPP, as shown in Figure 5, the anticyclone over the Yellow Sea contributed to the transport of more CO from
177 China to the Korean Peninsula. Furthermore, high concentrations of CO in regions throughout China were observed. Thus, the
178 combination of these two effects led to model predictions of higher concentrations over Korea.

179

180 The raw hypothesis from Eulerian outputs is that a high CO concentration at a receptor during a specific period is due to LRT
181 from a source because the average wind moves toward the receptor during that period. This hypothesis is based on the average
182 wind speed and direction and the average CO concentration, which do not constitute a reliable source of this assumption. We
183 will briefly explain why we require merged output with simultaneous changes in trajectories and concentrations. To determine
184 the source of LRT, researchers should include one major parameter in their investigations: the trajectory of the air mass. Once
185 the location of the source and the trajectory of the air mass is known, the air mass is assumed to be polluted. If the air mass is
186 not polluted, then that source is not responsible for high concentrations in the receptor location. Therefore, linking the source
187 to the receptor based on only mean wind patterns and concentrations is not a reliable approach. The following paragraphs will
188 discuss how we combine concentrations and trajectories into one set of outputs to better explain the trajectories.

189 **4 Analysis of C-TRAIL**

190 Because C-TRAIL is a diagnostic tool derived from CMAQ, both a Lagrangian output and CMAQ standard Eulerian output
191 are available after each run. The C-TRAIL helps us identify the source-receptor linkage, save the full trajectory of packets,
192 and display the path of selected packets. Therefore, not only do C-TRAIL simulations provide all spatial concentration changes,
193 but they also display the trajectories of each packet, owing to the Lagrangian approach of TG. In addition, we are able to
194 determine changes in concentrations along this trajectory. The difference between this model and other meteorological-based
195 models is that they enable us to study changes in the concentrations of selected species along different paths, investigate the
196 evidence for the amount of pollution in originated air masses, study the reason behind the oscillation of concentrations, and
197 examine the linkage of oscillations to both sources and sinks along the path.

198 This section provides an example of how we use C-TRAIL to study the sources of different packets from different altitudes
199 (from below 1 km to almost 10 km) over the Seoul Metropolitan Area (SMA); later sections will focus on the entire month of
200 May 2016 C-TRAIL over the SMA and provide more comprehensive illustrations of the concentrations and altitudes of
201 trajectories. Figure 6 displays the C-TRAIL output for June 4, 2016. We gathered all of the packets over the city of Seoul and
202 analyzed the trajectory of each packet. Figure 6(a) shows the path of all the packets from their sources. Packets are represented
203 by different colors. We observed that some of the packets came from southeastern South Korea, and one originated in
204 southeastern China, traveled over the Yellow Sea, and landed in Seoul. Some of the packets also originated northwest of South
205 Korea from northern China. Most of the packets, however, were locally initiated, generally from regions around the SMA.
206 Using the HYSPLIT back-trajectory model, we found relatively similar trajectories (Figure S6).

208
209 Figure 6(b) depicts how the CO concentration of the four most aged packets changed as they traveled on their path toward
210 Seoul. This type of output is a new feature and has not been studied before. With meteorological-based back-trajectory models,
211 the path of air parcels and their back trajectories can be delineated; we are the first, however, to use a CMAQ-based Lagrangian

212 integrated model to study the concentrations of species (in this case, CO) via the paths of air packets. The four most aged
213 packets came from 24, 21, 20, and 17 times step back (Figure 6(b)). We find these packets interesting because they follow a
214 long path, changes in their concentrations fluctuate, and they are easy to comprehend. From studying these packets and their
215 C-TRAILs, we generally understand that the concentration of each packet increases as it approaches the SMA. The
216 concentrations of near-surface packets tend to fluctuate more than those of high-altitude packets (Figure S7). Also, larger
217 oscillations in the concentrations occur over land rather than over the ocean, which, however, becomes more vivid when a
218 near-surface packet reaches land from the ocean and suddenly peaks in concentration. The sudden peaks of concentrations of
219 near-surface packets are due to their movement over either a city or some source of emissions. Over the SMA and other cities,
220 two peaks, mainly caused by on-road emissions, occur during local morning and evening times.

221 5 Case Study for the C-TRAIL Analysis: The May 2016 KORUS-AQ Period

222 Using a conventional method with model data gathered over the course of a month or a year to incorporate concentrations into
223 a trajectory analysis produces a tremendous amount of outputs, making all outputs difficult to interpret simultaneously. For
224 our case study, covering May 2016, we selected Seoul, South Korea, over East Asia as the receptor. We plotted C-TRAIL
225 outputs according to variations in the packet concentrations and their distances from the receptor. **Error! Reference source**
226 **not found.**(a) presents the general path of all packet trajectories reaching the Seoul area at different altitudes at 9:00 AM LT
227 throughout May 2016. The color bar represents the altitude at which the packets were traveling. Generally, packets at low
228 altitudes traveled from local areas to Seoul, and those at high altitudes traveled from more distant regions. One exception was
229 packets that originated in the Shandong Peninsula; some traveled at high altitudes and some at low altitudes. **Error! Reference**
230 **source not found.**(b) displays a C-TRAIL that represented a unique type of packet that followed the concentrations of
231 trajectories. In this case, each packet at each location (or hour of the trajectory) had a specific CO concentration that depended
232 on its altitude (high altitude/surface), its location (land/sea/urban/forest), and the hour of the day (traffic hours/non-traffic
233 hours). To better explain the location of packets and the variability in their trajectory paths before reaching Seoul, we created
234 a boxplot, shown in **Error! Reference source not found.**(c), of packet distances in kilometers from the receptor at each hour
235 before the packets reached Seoul. When the packets reached Seoul at 9:00 AM local time, the distance became zero.
236 Furthermore, the boxplot of trajectories' heights for all the periods is presented in Fig. S8. In a study of C-TRAIL outputs, it
237 is better to account for trajectories, concentrations, and distances simultaneously. As a result, the concentrations and distances
238 of packets in early hours (10:00 AM to 2:00 PM of local time) in **Error! Reference source not found.** show high variability
239 in concentrations with a median of around 150 ppbv and a maximum as high as 500 ppbv. Most of these packets originated far
240 from the receptor (i.e., eastern, northern, and southeastern China). The median of the concentration shown in the boxplot rose
241 slightly between 6:00 PM and 10:00 PM. Distances also showed more variation during this period, which can be explained
242 by the different paths of the trajectories (i.e., local trajectories with shorter distances and LRT trajectories with longer
243 distances). As the packets approached Seoul (6:00 AM to 9:00 AM), the upper whisker of concentration values increased to

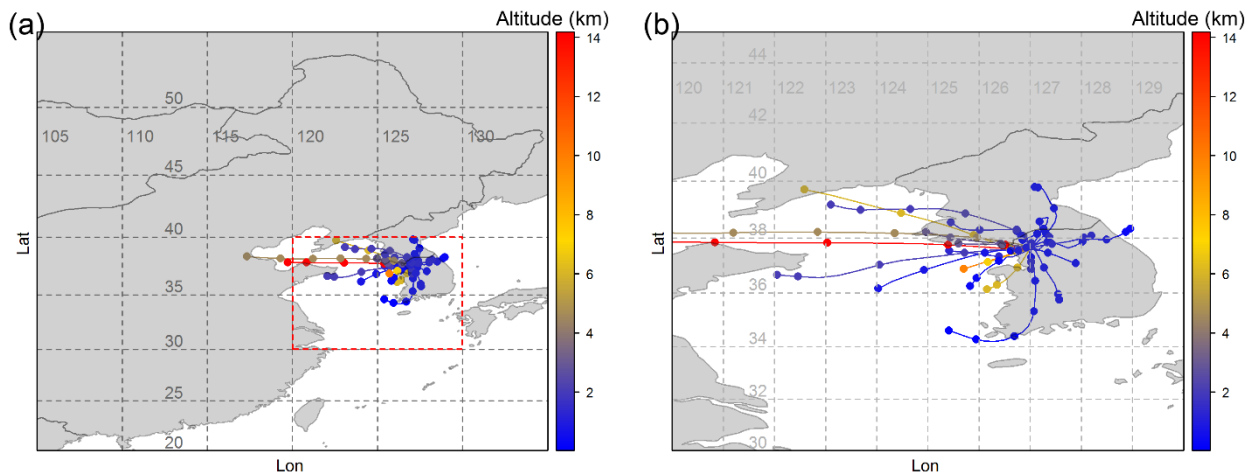
244 as high as 400 ppbv, and the distances approached zero, indicating higher concentrations of CO over local trajectories resulting
245 from surface on-road emissions and other emission sources.

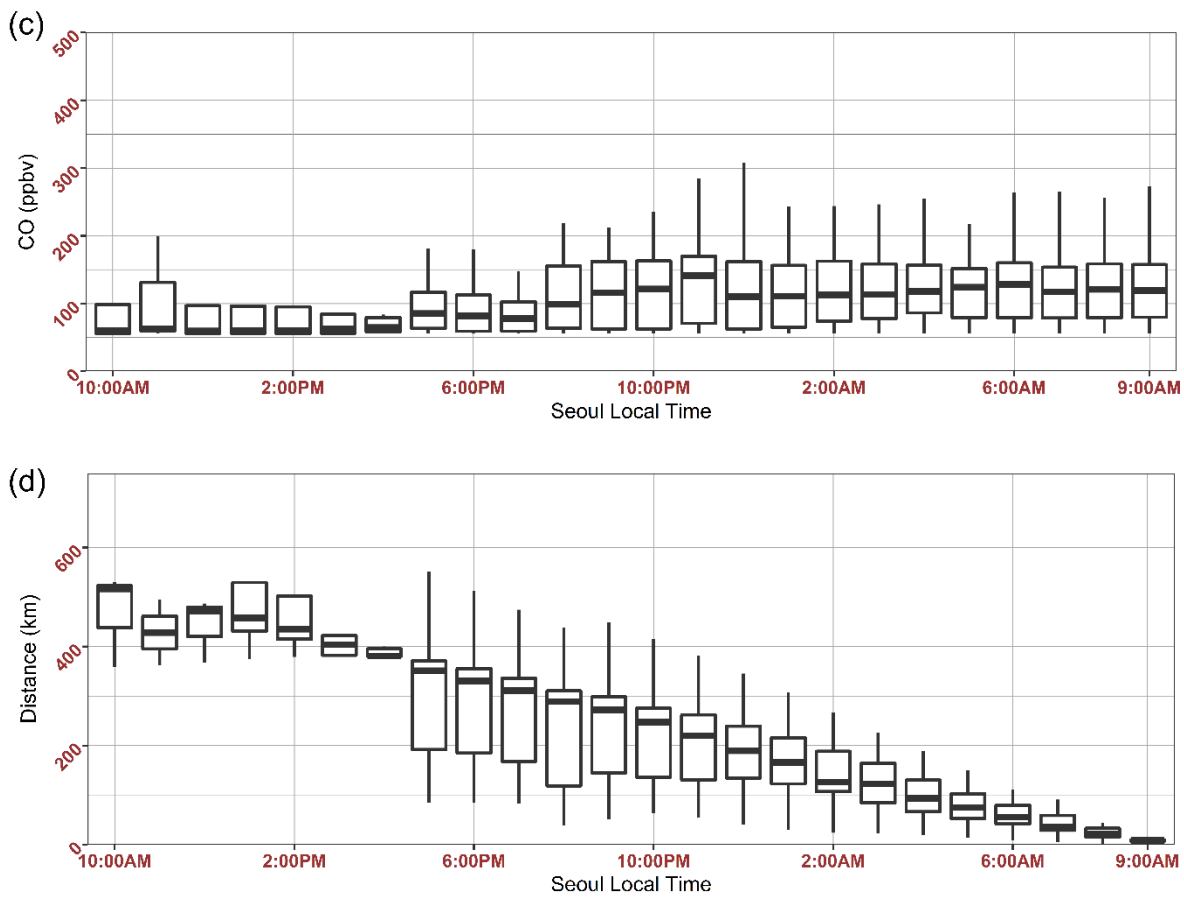
246

247 Because of variable weather and wind (i.e., cloudy, rainy, or clear) during the DWP, C-TRAIL showed a mixed response of
248 trajectories from both local and long-range transport, shown in Figure 8(a). A wide interquartile range and a median of close
249 to the 25th percentile at 11:00 AM and 12:00 PM indicate that a few packets contained high concentrations of CO (close to
250 300 ppbv), but the majority consisted of low concentrations (around 100 ppbv). The distance output of low-concentration
251 packets showed distances as long as 500 km (over the Shandong Peninsula). As the packets approached Seoul, the median
252 concentration values were as high as 150 ppbv. Thus, from Figure 8, we conclude that most of the long trajectories followed
253 a path at high altitudes (higher than 7 km), and the polluted trajectories, which originated in the Shandong Peninsula, were
254 from the near-surface, shown in Figure 8(a).

255

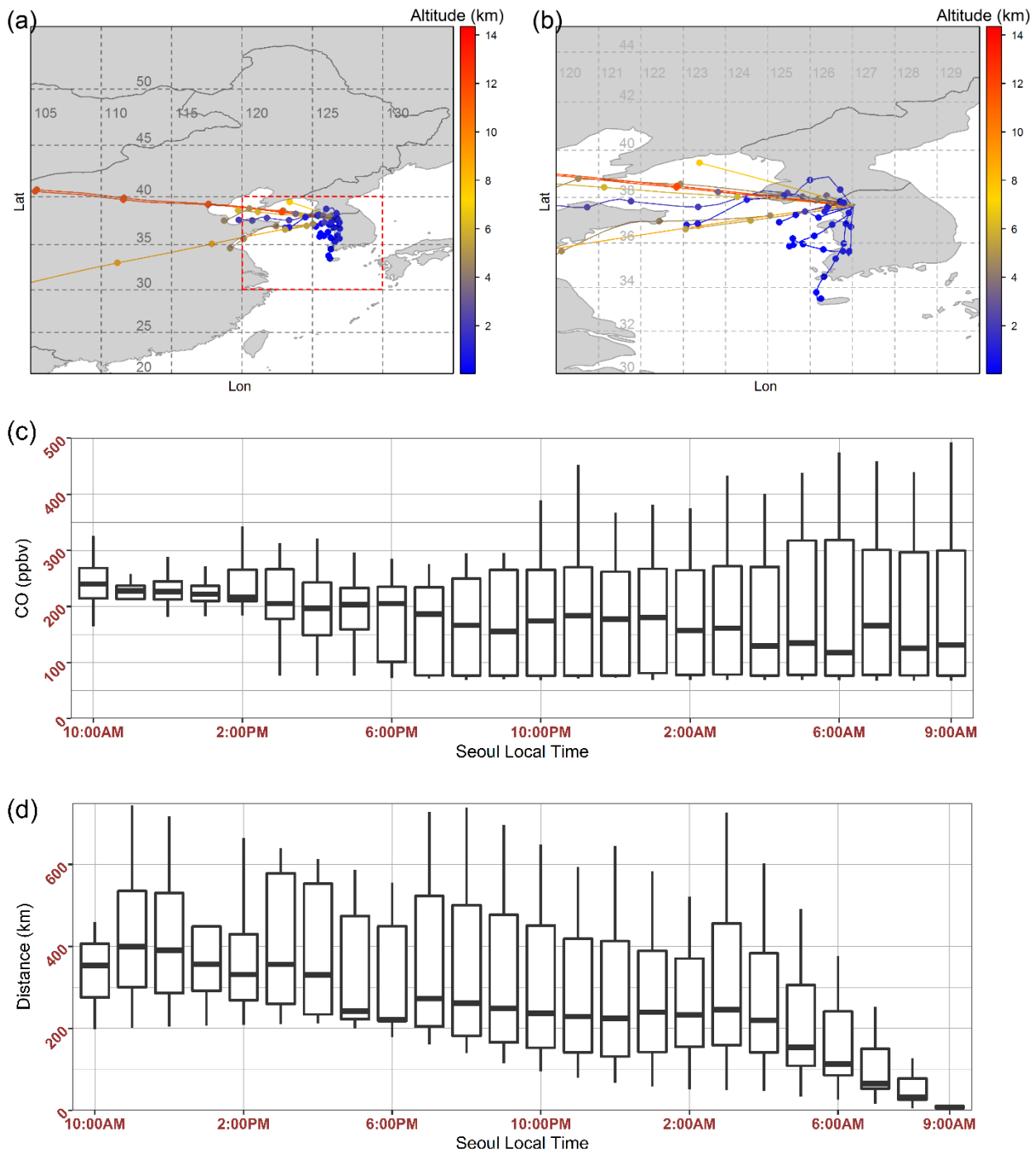
256 Unlike the DWP, the SP showed a more vivid display of trajectories, nearly all of which could be considered local trajectories.
257 Long-range trajectories could not be considered responsible for the CO concentration values of Seoul. After all, from 10:00
258 AM to 4:00 PM (





259 Figure 9(a) and (b)), nearly all of the long-distance packets had concentrations of less than 100 ppbv. The local origination of
 260 highly polluted trajectories can be explained by a high-pressure system over the Korean Peninsula during this period, which
 261 was responsible for very low wind speeds. The poor emission inventory over East Asia, however, provided extreme under-
 262 predictions of high concentration values during this period. Therefore, when studying model outputs, we should account for
 263 various aspects of the model (e.g., the transport, diffusion, formation, deposition, and convention), in which diffusion, in this
 264 case, played a significant role in CO concentration values at the receptor location.

265
 266 During the EPP, several high concentrations of CO appeared at the early points of trajectories. These high concentrations,
 267 combined with high distance values, indicate that the LRT of polluted air masses was responsible for high concentrations of
 268 CO during this period (



269 Figure 10). Furthermore, the variability of CO concentrations from 10:00 PM to 9:00 AM at the receptor location stemmed
270 from both the various paths of the trajectories and the distances. The high concentration trajectories close to the surface, which
271 originated in the Shandong Peninsula, passed over the Yellow Sea and landed in Seoul at 9:00 AM. When the surface packets

272 reached urban areas, they presented maximum CO concentrations, depending on the time of day and the rush-hour traffic. An
273 assumption made by studies that used Eulerian model outputs or meteorological-based Lagrangian models for this period was
274 that transport played an important role (Lee et al., 2019). The outputs from C-TRAIL also indicate that highly polluted air
275 masses originated in China (the source) and landed in Seoul (the receptor). That is, the findings of this study regarding the
276 trajectories and the origin of polluted air masses are similar to those of previous studies.

277
278 We further analyzed the diverse aspects of C-TRAIL results using the Open-air package in R (Carslaw and Ropkins, 2012)
279 and determined the frequency of trajectories passing through every one-degree by one-degree gridded area, illustrated in Figure
280 11(a). Central China, northern China, and North Korea were not common areas for packet movement because the packets most
281 likely passed only once through the grids of these regions (at a frequency of about one percent). For the Yellow Sea and the
282 Shandong Peninsula region, however, trajectories more likely passed at a frequency of about ten percent. The figure also
283 shows that most of the trajectories (25 to 100 percent) passed over the west side of the SMA, a two-degree by two-degree area
284 (the dark red section in Figure 11 (a)). We can classify trajectories into separate segments according to their concentrations.
285 Figure 11(b) shows this type of classification and the link between the average concentration of all trajectories to their paths.
286 While higher concentrations were most likely the result of local transport, lower concentrations were most likely from LRT.
287 For the May 2016 case, while most of the high concentration values corresponded to packets that originated in South Korea or
288 close to the SMA, most of the low concentration values corresponded to packets originating in China: their impact, however,
289 is still evident.

290
291 By clustering the outputs of C-TRAIL, we are better able to locate the dominant paths for the May 2016 trajectories. According
292 to Figure 12(a), based on the Euclidean distance function, about 37.8% of trajectories originated in local areas east, south, and
293 north of the SMA. About 16.1% of trajectories originated in northern China and followed paths over the Yellow Sea to the
294 SMA; about 10.5% of the trajectories came from southwestern South Korea and traveled over the Yellow Sea to reach the
295 SMA; about 21.3% of trajectories came from the Shandong Peninsula, and the remaining trajectories (5.3%) originated in
296 central China and were transported over China and the Yellow Sea to the SMA. Angle clustering in Figure 12(b), however,
297 tells a different story about the trajectories. Clustering by the angle distance function shows a similarity among the angles from
298 the starting points of the back trajectories. Generally, nearly all of the packets originated on the west side of the SMA, 32.2%
299 farther west, 34.5% in the southwest, 12.7% in the south/south-west, 14.9% in the northwest, and 5.7% in the east/southeast.
300 This clustering is consistent with strong westerly winds during the spring in East Asia.

301
302 By quantifying clusters based on their trajectories, cluster analyses show the relative importance of regional sources.
303 Nevertheless, they are not completely accurate at determining the relative contribution of potential source regions because they
304 do not consider concentrations along with trajectories. One method of calculating the probability of potential sources is the
305 potential source contribution function (PSCF), which finds the probability that a source is located at a specific latitude and

306 longitude (Pekney et al., 2006). Figure 12(c) shows that the probability of packets with high concentrations (i.e., those with
307 concentrations at or above 90 percentile) passing over the Yellow Sea and reaching the SMA from the southwest was higher
308 than 0.3. Two areas through which one packet containing a high concentration of pollutants passed showed a high probability
309 of 0.6 and 0.5. One was southwest of the SMA over the Yellow Sea and the other between North Korea and the coast of
310 northern China over the Yellow Sea.

311

312 One important limitation of the PSCF is its complexity distinguishing between moderate and strong sources. To overcome this
313 problem, we can apply the concentration-weighted trajectory (CWT) method to compute concentration fields for identifying
314 strong source areas of pollutants. The CWT method, based on concentration values over each trajectory, estimates the trajectory
315 weighted concentration in each grid cell by averaging the sample pollutant concentrations of trajectories crossing each grid
316 cell (one degree by one degree)—the results of CWT show close agreement with those of the PSCF. Figure 12(d) shows the
317 distribution of weighted trajectory concentrations of CO in May 2016 surrounding the SMA. The CWT results show that not
318 only were the Yellow Sea and the Shandong Peninsula potential sources of high concentration over the SMA, but other local
319 sources may also have been strong sources. For example, the Pyongyang area in North Korea had a high concentration,
320 weighted over 250 ppb, indicating a strong potential source of CO in this month. Furthermore, local regions such as that west,
321 east, and south of the SMA showed a strong potential source of high CO concentration in Seoul. Among the long-distance
322 sources, only the Shandong Peninsula and some parts of northern China had CO concentrations of around 100 ppmV according
323 to the CWT analysis. As other long-distance sources were not strong sources because of the scarcity of trajectories in these
324 areas, we consider them rare sources. For instance, although the LRT explained the high CO concentrations over the SMA
325 during the extreme pollution period (May 25-28), during longer periods (e.g., one month or one year), with a similar
326 contribution, distant regions from the SMA may not have been strong sources.

327

328 6 Conclusion

329 In this study, we introduced Lagrangian output, C-TRAIL, extracted from the Eulerian CMAQ model. The C-TRAIL
330 comprehensive output directly linked the trajectories of pollution from the source to the receptor. We used concentration and
331 trajectory values of C-TRAIL outputs to investigate the pollution status of originated air masses by classifying the outputs
332 from May 2016 over East Asia into separate categories. Unlike the conventional Eulerian CO concentration plots for separate
333 periods, which did not exhibit a clear relationship between the source and the receptor, the C-TRAIL outputs, which combined
334 trajectories and concentrations, accurately determined the impact of LRT on pollution during the EPP. Furthermore, during
335 the dynamic weather period, C-TRAIL outputs showed that polluted packets from the Shandong Peninsula were responsible
336 for high CO concentrations. The outputs for the SP revealed CO concentrations of less than 100 ppbv for distant packets,
337 strong evidence supporting the link between local trajectories and CO concentrations over the SMA during this period.

338

339 More comprehensive investigations on C-TRAIL outputs found that the Shandong Peninsula, local regions near the SMA, and
340 the Pyongyang area were potentially strong sources of CO pollutants during the entire month of May 2016. Overall, by
341 analyzing the trajectory paths of packets that reached in specific locations, we were able to generalize that C-TRAIL represents
342 an ideal tool for ascertaining the impact of long-range transport on species concentrations over a receptor by simultaneously
343 providing concentrations and trajectories. C-TRAIL can be applied to LRT-impacted regions such as East Asia, North
344 America, and India. Owing to the uncertainties inherent to emission inventories and immature diffusion modeling methods,
345 however, C-TRAIL outputs may have limitations that we will address in future work. The objective of this study is to suggest
346 an effective tool for establishing a link between real sources of pollution to a receptor via trajectory analysis. The results of
347 this study over East Asia showed the reliability and various advantages of C-TRAIL output. Therefore, because of its capability
348 to determine the trajectories of masses of CO concentrations with high computational efficiency, C-TRAIL output could prove
349 to be a highly useful tool for those who model air quality over a specific region and investigate sources of polluted air masses.
350

351 **Code Availability.** The C-TRAIL version 1.0 is available for non-commercial research purposes at
352 <https://github.com/armanpouyaei/C-TRAIL-v1.0>.

353

354 **Supplement.** A supplementary document related to this article follows.

355

356 **Author Contribution.** A. P., Y. C. and B. S. contributed to the design and implementation of the research. J. J. prepared the
357 CMAQ model and inputs. A. P. prepared the model, analyzed the results, and took the lead in writing the manuscripts. Y. C.
358 and C. H. S. supervised the project. All authors discussed the results and commented on the manuscript and contributed to the
359 final version of the manuscript.

360

361 **Competing interest.** The authors declare no competing financial and/or non-financial interests in relation to the work
362 described.

363

364 **Acknowledgments.** We wish to acknowledge Dr. Peter Percell for his technical support in the development of CMAQ-TG in
365 this research. This study was funded by the National Strategic Project-Fine particle of the National Research Foundation of
366 Korea (NRF) funded by the Ministry of Science and ICT (MSIT), the Ministry of Environment (ME), and the Ministry of
367 Health and Welfare (MOHW) (NRF-2017M3D8A1092022).

368 **7 References**

369 Al-Saadi, J., Carmichael, G., Crawford, J., Emmons, L., Kim, S., Song, C.-K., Chang, L.-S., Lee, G., Kim, J. and Park, R.:
370 KORUS-AQ: An International Cooperative Air Quality Field Study in Korea (2016). [online] Available from:
371 <https://espo.nasa.gov/korus-aq/content/KORUS-AQ>, 2016.

372 Bertschi, I. T. and Jaffe, D. A.: Long-range transport of ozone, carbon monoxide, and aerosols to the NE Pacific troposphere
373 during the summer of 2003: Observations of smoke plumes from Asian boreal fires, *J. Geophys. Res. D Atmos.*, 110(5), 1–14,
374 doi:10.1029/2004JD005135, 2005.

375 Byun, D. and Schere, K. L.: Review of the governing equations, computational algorithms, and other components of the
376 models-3 Community Multiscale Air Quality (CMAQ) modeling system, *Appl. Mech. Rev.*, 59(1–6), 51–76,
377 doi:10.1115/1.2128636, 2006.

378 Carroll, M., Ocko, I. B., McNeal, F., Weremijewicz, J., Hogg, A. J., Opoku, N., Bertman, S. B., Neil, L., Fortner, E.,
379 Thornberry, T., Town, M. S., Yip, G. and Yageman, L.: An Assessment of Forest Pollutant Exposure Using Back Trajectories,
380 Anthropogenic Emissions, and Ambient Ozone and Carbon Monoxide Measurements, *Am. Geophys. Union, Fall Meet.* 2008,
381 Abstr. id. A41H-0227, 2008.

382 Carslaw, D. C. and Ropkins, K.: Openair - An r package for air quality data analysis, *Environ. Model. Softw.*, 27–28, 52–61,
383 doi:10.1016/j.envsoft.2011.09.008, 2012.

384 Chen, T. F., Chang, K. H. and Tsai, C. Y.: Modeling direct and indirect effect of long range transport on atmospheric PM 2.5
385 levels, *Atmos. Environ.*, 89, 1–9, doi:10.1016/j.atmosenv.2014.01.065, 2014.

386 Chock, D. P., Sun, P. and Winkler, S. L.: Trajectory-grid: An accurate sign-preserving advection-diffusion approach for air
387 quality modeling, *Atmos. Environ.*, 30(6), 857–868, doi:10.1016/1352-2310(95)00332-0, 1996.

388 Chock, D. P., Whalen, M. J., Winkler, S. L. and Sun, P.: Implementing the trajectory-grid transport algorithm in an air quality
389 model, *Atmos. Environ.*, 39(22), 4015–4023, doi:10.1016/j.atmosenv.2005.03.037, 2005.

390 Choi, J., Park, R. J., Lee, H. M., Lee, S., Jo, D. S., Jeong, J. I., Henze, D. K., Woo, J. H., Ban, S. J., Lee, M. Do, Lim, C. S.,
391 Park, M. K., Shin, H. J., Cho, S., Peterson, D. and Song, C. K.: Impacts of local vs. trans-boundary emissions from different
392 sectors on PM2.5 exposure in South Korea during the KORUS-AQ campaign, *Atmos. Environ.*, 203, 196–205,
393 doi:10.1016/j.atmosenv.2019.02.008, 2019.

394 Choi, S. H., Ghim, Y. S., Chang, Y. S. and Jung, K.: Behavior of particulate matter during high concentration episodes in
395 Seoul, *Environ. Sci. Pollut. Res.*, 21(9), 5972–5982, doi:10.1007/s11356-014-2555-y, 2014.

396 Chuang, M. T., Fu, J. S., Jang, C. J., Chan, C. C., Ni, P. C. and Lee, C. Te: Simulation of long-range transport aerosols from
397 the Asian Continent to Taiwan by a Southward Asian high-pressure system, *Sci. Total Environ.*, 406(1–2), 168–179,
398 doi:10.1016/j.scitotenv.2008.07.003, 2008.

399 Chuang, M. T., Lee, C. Te and Hsu, H. C.: Quantifying PM2.5 from long-range transport and local pollution in Taiwan during
400 winter monsoon: An efficient estimation method, *J. Environ. Manage.*, 227(July), 10–22, doi:10.1016/j.jenvman.2018.08.066,

401 2018.

402 Cristofanelli, P., Bonasoni, P., Carboni, G., Calzolari, F., Casarola, L., Zauli Sajani, S. and Santaguida, R.: Anomalous high
403 ozone concentrations recorded at a high mountain station in Italy in summer 2003, *Atmos. Environ.*, 41(7), 1383–1394,
404 doi:10.1016/j.atmosenv.2006.10.017, 2007.

405 Döös, K., Jönsson, B. and Kjellsson, J.: Evaluation of oceanic and atmospheric trajectory schemes in the TRACMASS
406 trajectory model v6.0, *Geosci. Model Dev.*, 10(4), 1733–1749, doi:10.5194/gmd-10-1733-2017, 2017.

407 Draxler, R. R.: An overview of the HYSPLIT_4 modelling system for trajectories, dispersion and deposition, *Aust. Meteorol.*
408 *Mag.*, 47(4), 295–308, 1998.

409 Eslami, E., Salman, A. K., Choi, Y., Sayeed, A. and Lops, Y.: A data ensemble approach for real-time air quality forecasting
410 using extremely randomized trees and deep neural networks, *Neural Comput. Appl.*, doi:10.1007/s00521-019-04287-6, 2019.

411 Gratz, L. E., Jaffe, D. A. and Hee, J. R.: Causes of increasing ozone and decreasing carbon monoxide in springtime at the Mt.
412 Bachelor Observatory from 2004 to 2013, *Atmos. Environ.*, 109, 323–330, doi:10.1016/j.atmosenv.2014.05.076, 2015.

413 Halliday, H. S., DiGangi, J. P., Choi, Y., Diskin, G. S., Pusede, S. E., Rana, M., Nowak, J. B., Knot, C., Ren, X., He, H.,
414 Dickerson, R. R. and Li, Z.: Using Short-Term CO/CO 2 Ratios to Assess Air Mass Differences over the Korean Peninsula
415 during KORUS-AQ, *J. Geophys. Res. Atmos.*, 1–22, doi:10.1029/2018jd029697, 2019.

416 Heald, C. C., Jacob, D. J., Fiore, A. M., Emmons, L. K., Gille, J. C., Deeter, M. N., Warner, J., Edwards, D. P., Crawford, J.
417 H., Hamlin, A. J., Sachse, G. W., Browell, E. V., Avery, M. A., Vay, S. A., Westberg, D. J., Blake, D. R., Singh, H. B.,
418 Sandholm, S. T., Talbot, R. W. and Fuelberg, H. E.: Asian outflow and trans-Pacific transport of carbon monoxide and ozone
419 pollution: An integrated satellite, aircraft, and model perspective, *J. Geophys. Res. D Atmos.*, 108(24),
420 doi:10.1029/2003jd003507, 2003.

421 Hu, Y. and Talat Odman, M.: A comparison of mass conservation methods for air quality models, *Atmos. Environ.*, 42(35),
422 8322–8330, doi:10.1016/j.atmosenv.2008.07.042, 2008.

423 Jeon, W., Choi, Y., Percell, P., Hossein Souri, A., Song, C. K., Kim, S. T. and Kim, J.: Computationally efficient air quality
424 forecasting tool: Implementation of STOPS v1.5 model into CMAQ v5.0.2 for a prediction of Asian dust, *Geosci. Model Dev.*,
425 9(10), 3671–3684, doi:10.5194/gmd-9-3671-2016, 2016.

426 Jung, J., Souri, A. H., Wong, D. C., Lee, S., Jeon, W., Kim, J. and Choi, Y.: The Impact of the Direct Effect of Aerosols on
427 Meteorology and Air Quality Using Aerosol Optical Depth Assimilation During the KORUS-AQ Campaign, *J. Geophys. Res.*
428 *Atmos.*, 124(14), 8303–8319, doi:10.1029/2019jd030641, 2019.

429 Kruse, S., Gerdes, A., Kath, N. J. and Herzschuh, U.: Implementing spatially explicit wind-driven seed and pollen dispersal in
430 the individual-based larch simulation model: LAVESI-WIND 1.0, *Geosci. Model Dev.*, 11(11), 4451–4467, doi:10.5194/gmd-
431 11-4451-2018, 2018.

432 Lee, S., Ho, C. H. and Choi, Y. S.: High-PM10 concentration episodes in Seoul, Korea: Background sources and related
433 meteorological conditions, *Atmos. Environ.*, 45(39), 7240–7247, doi:10.1016/j.atmosenv.2011.08.071, 2011.

434 Lee, S., Ho, C. H., Lee, Y. G., Choi, H. J. and Song, C. K.: Influence of transboundary air pollutants from China on the high-

435 PM10 episode in Seoul, Korea for the period October 16-20, 2008, *Atmos. Environ.*, 77, 430–439,
436 doi:10.1016/j.atmosenv.2013.05.006, 2013.

437 Lee, S., Kim, J., Choi, M., Hong, J., Lim, H., Eck, T. F., Holben, B. N., Ahn, J. Y., Kim, J. and Koo, J. H.: Analysis of long-
438 range transboundary transport (LRTT) effect on Korean aerosol pollution during the KORUS-AQ campaign, *Atmos. Environ.*,
439 204(February), 53–67, doi:10.1016/j.atmosenv.2019.02.020, 2019.

440 Li, M., Zhang, Q., Kurokawa, J. I., Woo, J. H., He, K., Lu, Z., Ohara, T., Song, Y., Streets, D. G., Carmichael, G. R., Cheng,
441 Y., Hong, C., Huo, H., Jiang, X., Kang, S., Liu, F., Su, H. and Zheng, B.: MIX: A mosaic Asian anthropogenic emission
442 inventory under the international collaboration framework of the MICS-Asia and HTAP, *Atmos. Chem. Phys.*, 17(2), 935–
443 963, doi:10.5194/acp-17-935-2017, 2017.

444 Liu, Y., Xu, S., Ling, T., Xu, L. and Shen, W.: Heme oxygenase/carbon monoxide system participates in regulating wheat
445 seed germination under osmotic stress involving the nitric oxide pathway, *J. Plant Physiol.*, 167(16), 1371–1379,
446 doi:10.1016/j.jplph.2010.05.021, 2010.

447 Lops, Y., Choi, Y., Eslami, E. and Sayeed, A.: Real-time 7-day forecast of pollen counts using a deep convolutional neural
448 network, *Neural Comput. Appl.*, 1–10, doi:10.1007/s00521-019-04665-0, 2019.

449 Miyazaki, K., Sekiya, T., Fu, D., Bowman, K. W., Kulawik, S. S., Sudo, K., Walker, T., Kanaya, Y., Takigawa, M., Oogochi,
450 K., Eskes, H., Boersma, K. F., Thompson, A. M., Gaubert, B., Barre, J. and Emmons, L. K.: Balance of Emission and
451 Dynamical Controls on Ozone During the Korea-United States Air Quality Campaign From Multiconstituent Satellite Data
452 Assimilation, *J. Geophys. Res. Atmos.*, 124(1), 387–413, doi:10.1029/2018JD028912, 2019.

453 Oh, H. R., Ho, C. H., Kim, J., Chen, D., Lee, S., Choi, Y. S., Chang, L. S. and Song, C. K.: Long-range transport of air
454 pollutants originating in China: A possible major cause of multi-day high-PM10 episodes during cold season in Seoul, Korea,
455 *Atmos. Environ.*, 109, 23–30, doi:10.1016/j.atmosenv.2015.03.005, 2015.

456 Pekney, N. J., Davidson, C. I., Zhou, L. and Hopke, P. K.: Application of PSCF and CPF to PMF-Modeled Sources of PM_{2.5}
457 in Pittsburgh, *Aerosol Sci. Technol.*, 40(10), 952–961, doi:10.1080/02786820500543324, 2006.

458 Petetin, H., Beekmann, M., Sciare, J., Bressi, M., Rosso, A., Sanchez, O. and Ghersi, V.: A novel model evaluation approach
459 focusing on local and advected contributions to urban PM2.5 levels - Application to Paris, France, *Geosci. Model Dev.*, 7(4),
460 1483–1505, doi:10.5194/gmd-7-1483-2014, 2014.

461 Price, H. U., Jaffe, D. A., Cooper, O. R. and Doskey, P. V.: Photochemistry, ozone production, and dilution during long-range
462 transport episodes from Eurasia to the northwest United States, *J. Geophys. Res. D Atmos.*, 109(23), 1–10,
463 doi:10.1029/2003JD004400, 2004.

464 Pu, W., Zhao, X., Shi, X., Ma, Z., Zhang, X. and Yu, B.: Impact of long-range transport on aerosol properties at a regional
465 background station in Northern China, *Atmos. Res.*, 153, 489–499, doi:10.1016/j.atmosres.2014.10.010, 2015.

466 Rößler, T., Stein, O., Heng, Y., Baumeister, P. and Hoffmann, L.: Trajectory errors of different numerical integration schemes
467 diagnosed with the MPTRAC advection module driven by ECMWF operational analyses, *Geosci. Model Dev.*, 11(2), 575–
468 592, doi:10.5194/gmd-11-575-2018, 2018.

469 Sadeghi, B., Choi, Y., Yoon, S., Flynn, J., Kotsakis, A. and Lee, S.: The characterization of fine particulate matter downwind
470 of Houston: Using integrated factor analysis to identify anthropogenic and natural sources, *Environ. Pollut.*, 262, 114345,
471 doi:10.1016/j.envpol.2020.114345, 2020.

472 Salvador, P., Artíñano, B., Querol, X. and Alastuey, A.: A combined analysis of backward trajectories and aerosol chemistry
473 to characterise long-range transport episodes of particulate matter: The Madrid air basin, a case study, *Sci. Total Environ.*,
474 390(2–3), 495–506, doi:10.1016/j.scitotenv.2007.10.052, 2008.

475 Sarwar, G., Simon, H., Bhave, P. and Yarwood, G.: Examining the impact of heterogeneous nitryl chloride production on air
476 quality across the United States, *Atmos. Chem. Phys.*, 12(14), 6455–6473, doi:10.5194/acp-12-6455-2012, 2012.

477 Sayeed, A., Choi, Y., Eslami, E., Lops, Y., Roy, A. and Jung, J.: Using a deep convolutional neural network to predict 2017
478 ozone concentrations, 24 hours in advance, *Neural Networks*, 121, 396–408, doi:10.1016/j.neunet.2019.09.033, 2020.

479 Souri, A. H., Choi, Y., Li, X., Kotsakis, A. and Jiang, X.: A 15-year climatology of wind pattern impacts on surface ozone in
480 Houston, Texas, *Atmos. Res.*, 174–175, 124–134, doi:10.1016/j.atmosres.2016.02.007, 2016.

481 Stenke, A., Dameris, M., Grewe, V. and Garny, H.: Implications of lagrangian transport for simulations with a coupled
482 chemistry-climate model, *Atmos. Chem. Phys.*, 9(15), 5489–5504, doi:10.5194/acp-9-5489-2009, 2009.

483 Stohl, A.: Trajectory statistics - A new method to establish source-receptor relationships of air pollutants and its application to
484 the transport of particulate sulfate in Europe, *Atmos. Environ.*, 30(4), 579–587, doi:10.1016/1352-2310(95)00314-2, 1996.

485 Stohl, A.: Computation, accuracy and applications of trajectories- a review and bibliography, *Dev. Environ. Sci.*, 1(C), 615–
486 654, doi:10.1016/S1474-8177(02)80024-9, 2002.

487 Stohl, A. and Seibert, P.: Accuracy of trajectories as determined from the conservation of meteorological tracers, *Q. J. R.*
488 *Meteorol. Soc.*, 124(549), 1465–1484, doi:10.1002/qj.49712454907, 1998.

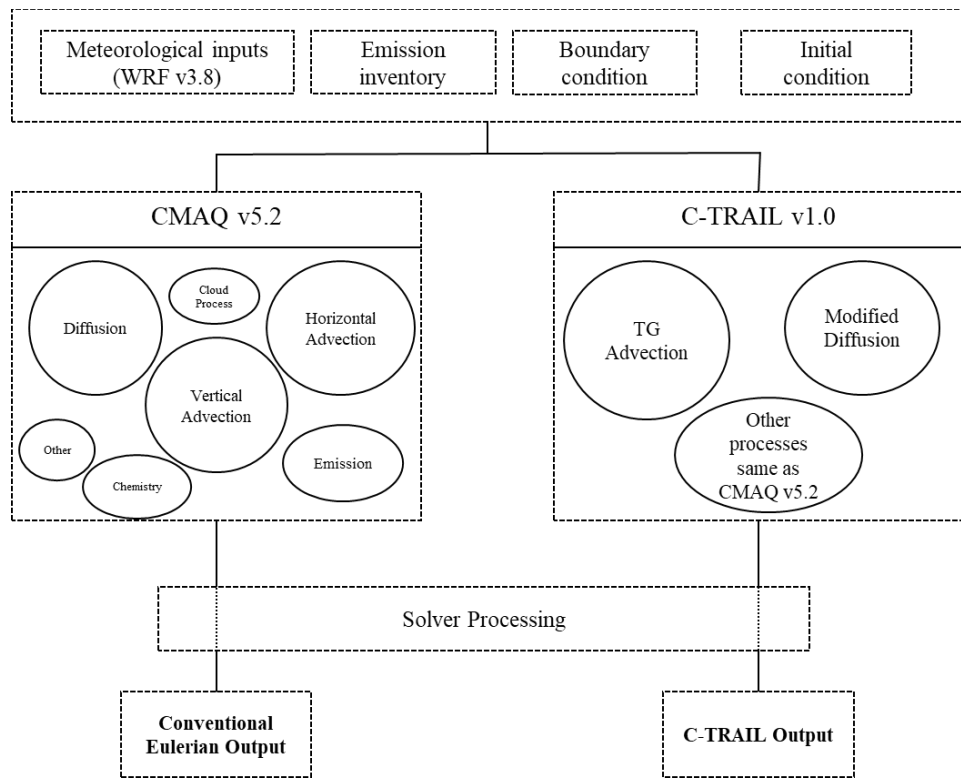
489 Vay, S. A., Choi, Y., Vadrevu, K. P., Blake, D. R., Tyler, S. C., Wisthaler, A., Hecobian, A., Kondo, Y., Diskin, G. S., Sachse,
490 G. W., Woo, J. H., Weinheimer, A. J., Burkhardt, J. F., Stohl, A. and Wennberg, P. O.: Patterns of CO<inf>2</inf> and
491 radiocarbon across high northern latitudes during International Polar Year 2008, *J. Geophys. Res. Atmos.*, 116(14), 1–22,
492 doi:10.1029/2011JD015643, 2011.

493 Wang, F., Chen, D. S., Cheng, S. Y., Li, J. B., Li, M. J. and Ren, Z. H.: Identification of regional atmospheric PM10 transport
494 pathways using HYSPLIT, MM5-CMAQ and synoptic pressure pattern analysis, *Environ. Model. Softw.*, 25(8), 927–934,
495 doi:10.1016/j.envsoft.2010.02.004, 2010.

496 Weiss-Penzias, P., Jaffe, D. A., Jaeglé, L. and Liang, Q.: Influence of long-range-transported pollution on the annual and
497 diurnal cycles of carbon monoxide and ozone at Cheeka Peak Observatory, *J. Geophys. Res. D Atmos.*, 109(23), 1–15,
498 doi:10.1029/2004JD004505, 2004.

499 Xu, S., Warner, N., Bohlin-Nizzetto, P., Durham, J. and McNett, D.: Long-range transport potential and atmospheric
500 persistence of cyclic volatile methylsiloxanes based on global measurements, *Chemosphere*, 228, 460–468,
501 doi:10.1016/j.chemosphere.2019.04.130, 2019.

502 Zhang, Q., Xue, D., Liu, X., Gong, X. and Gao, H.: Process analysis of PM 2.5 pollution events in a coastal city of China using

508 **Figure 1: Schematic of conventional CMAQ versus C-TRAIL**

1. Initialization

- Packets are generated based on the IC and BC in grid cells.
- Each packet receives an ID, x, y, z.
- Time-step selection is based on the condition that a packet may not travel more than $\frac{3}{4}$ of the distance between all opposite faces of a grid cell.

2. Packet Management

- The number of packets in each grid cell must not exceed five.
 - If exceeded:* Remove the extra packets.
The concentration of remaining packets will be the average of all available packets.
- Each grid cell must not be empty.
 - If empty:* Add an extra packet.
The concentration of the added packet will be similar to that of the closest packet.
- The properties of the packets are controlled through all time steps.

3. Advection

- The three-dimensional advection equation is solved to update the location of packets.

4. Diffusion

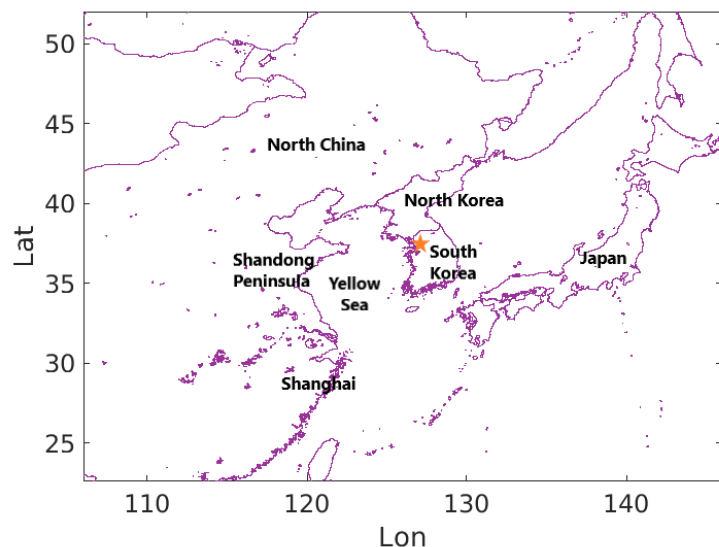
- The implicit Eulerian diffusion equation is solved to obtain an average over the number of packets in each grid cell.
- By considering each packet the center of the cell and the cell average as neighboring cells, the diffusion equation is solved for each packet using the predictor-corrector method.
- Horizontal diffusion requires extra sub-grid diffusion for pair-wise diffusion.

5. Emission

- The emission fluxes of various species (similar to CMAQ) are added to each packet through vertical diffusion.

6. Output Generation

- Based on Lambert's projection, the x, y, and z of each packet are converted into longitude, latitude, and altitude.
- C-TRAIL is generated during every output time step (1 hour).



515 **Figure 3: Domain of the study; the orange star indicates the Seoul Metropolitan Area (SMA)**

517

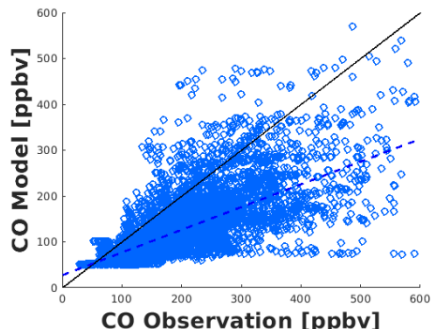
518 **Table 1: Comparison of the statistical parameters of CMAQ CO concentrations to aircraft measurements**
519 **(COR: correlation, IOA: index of agreement, RMSE: root mean square error, MAE: mean absolute error)**

		Abbreviation	COR	IOA	RMSE	MAE
a)	Entire month of May 2016		0.71	0.72	91.3	66.7
b)	Dynamic Weather Period	DWP	0.72	0.62	81.5	66.2
c)	Stagnant Period	SP	0.65	0.58	98.4	83.3
d)	Extreme Pollution Period	EPP	0.89	0.88	68.7	47.7

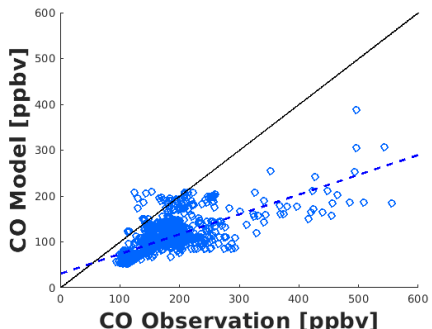
520

521

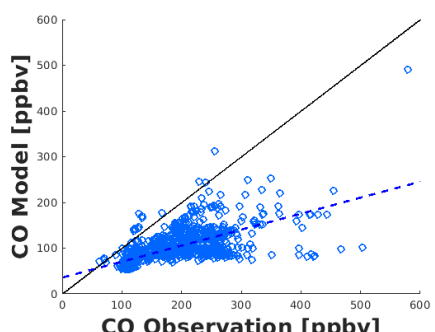
(a) Entire May 2016



(b) DWP



(c) SP



(d) EPP

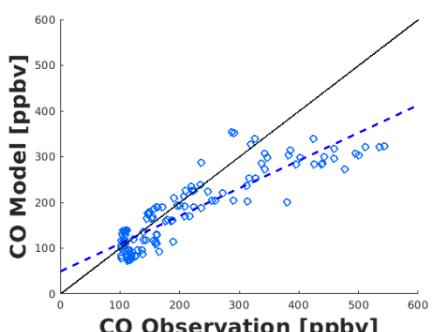
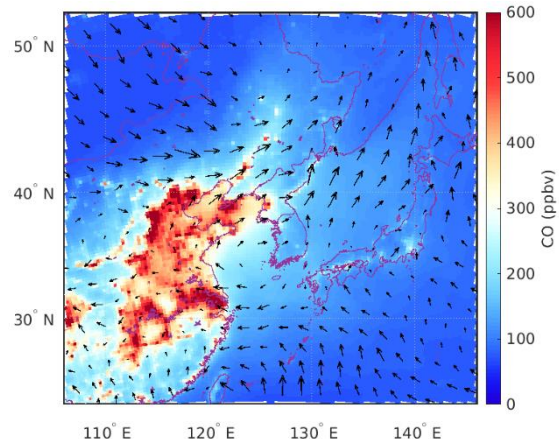
523
524

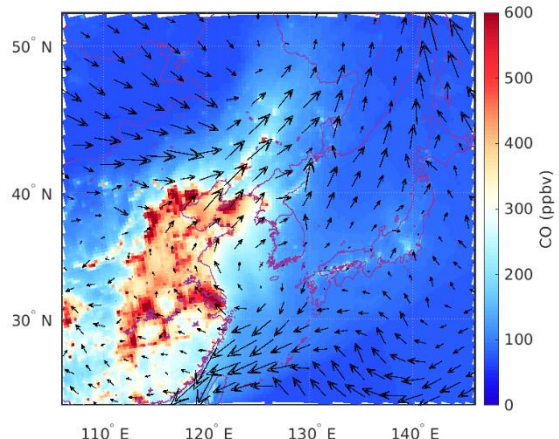
Figure 4: CMAQ model results versus aircraft CO measurements for (a) the entire month of May 2016 (n=6865),
 (b) the DWP (n=1750), (c) the SP (n=1548), and (d) the EPP (n=264)

525

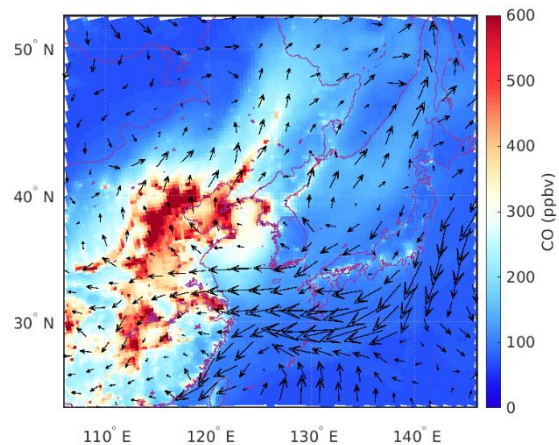
(a) An entire month of May 2016



(b) DWP



(c) SP



(d) EPP

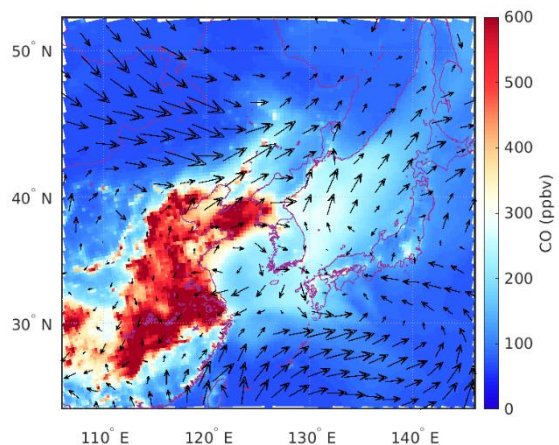
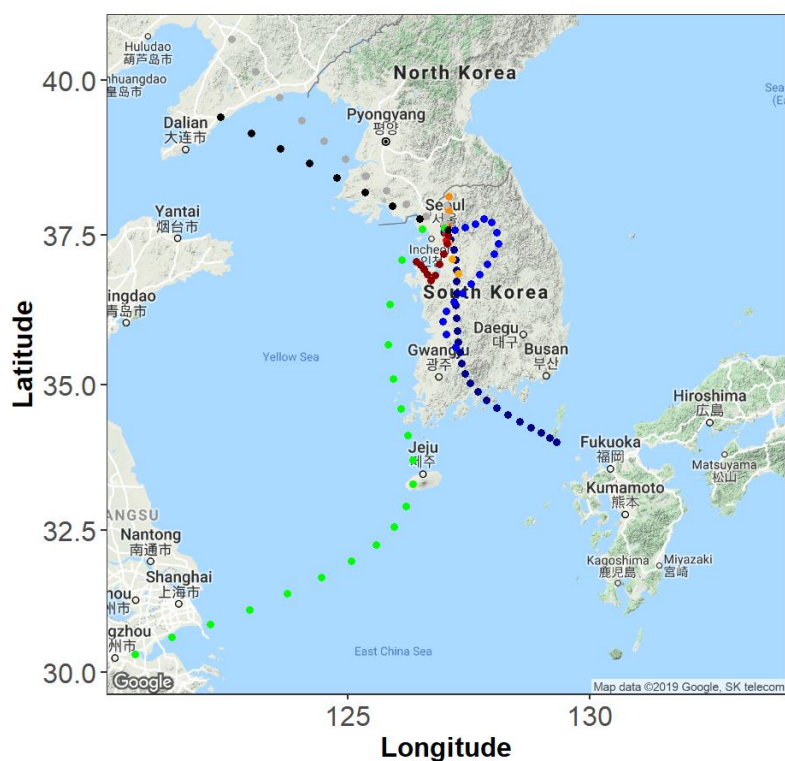
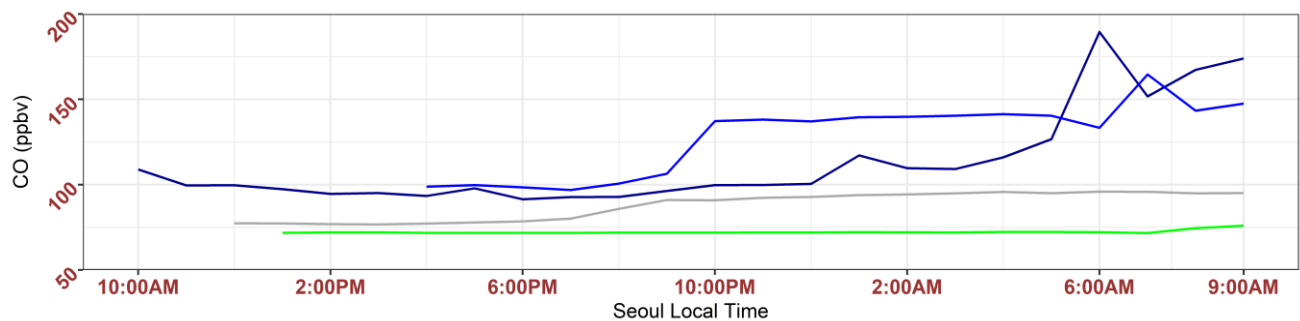


Figure 5: Model CO concentrations and wind patterns over the surface during (a) the entire month of May 2016, (b) the DWP, (c) the SP, and (d) the EPP

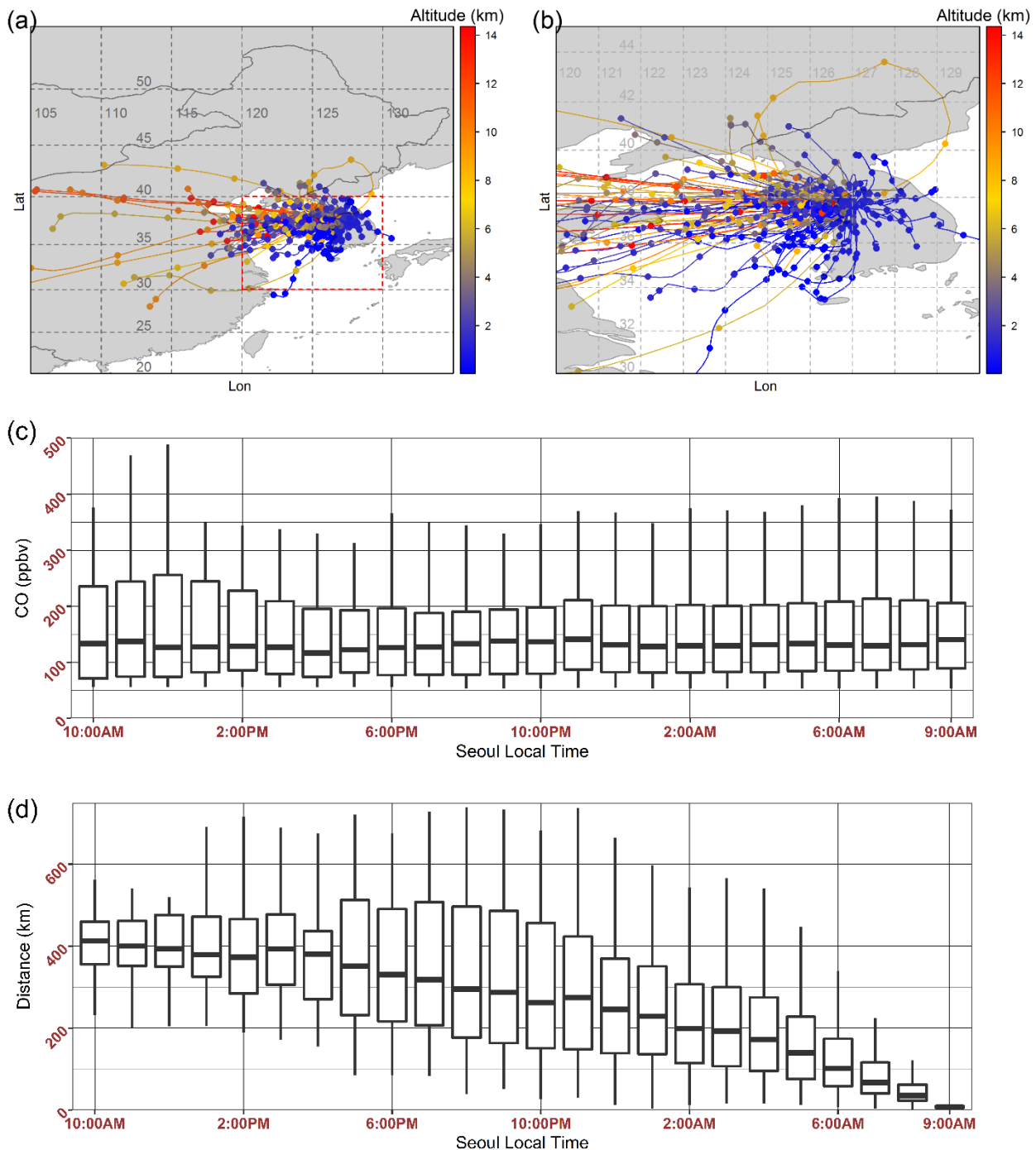
(a)



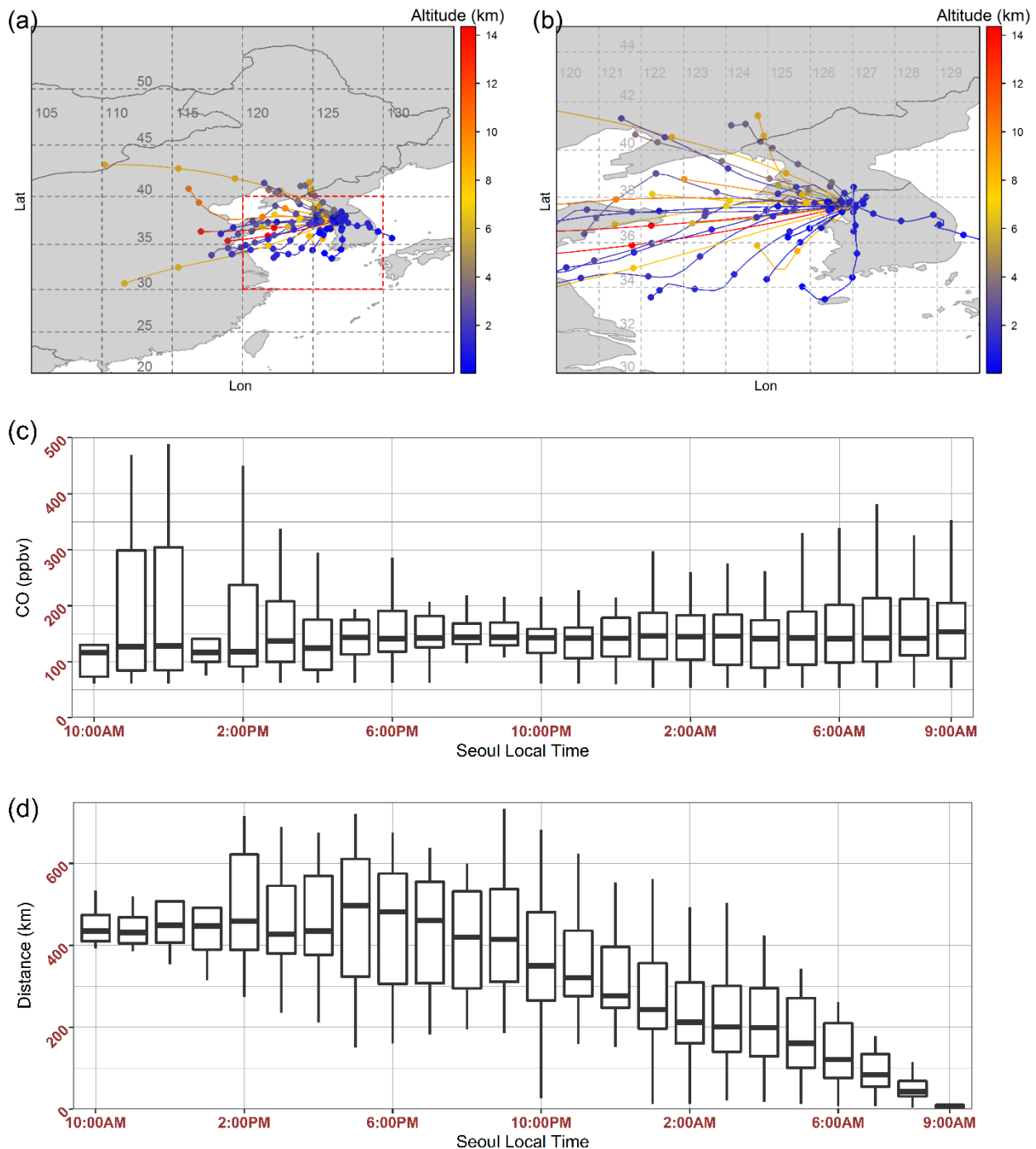
(b)



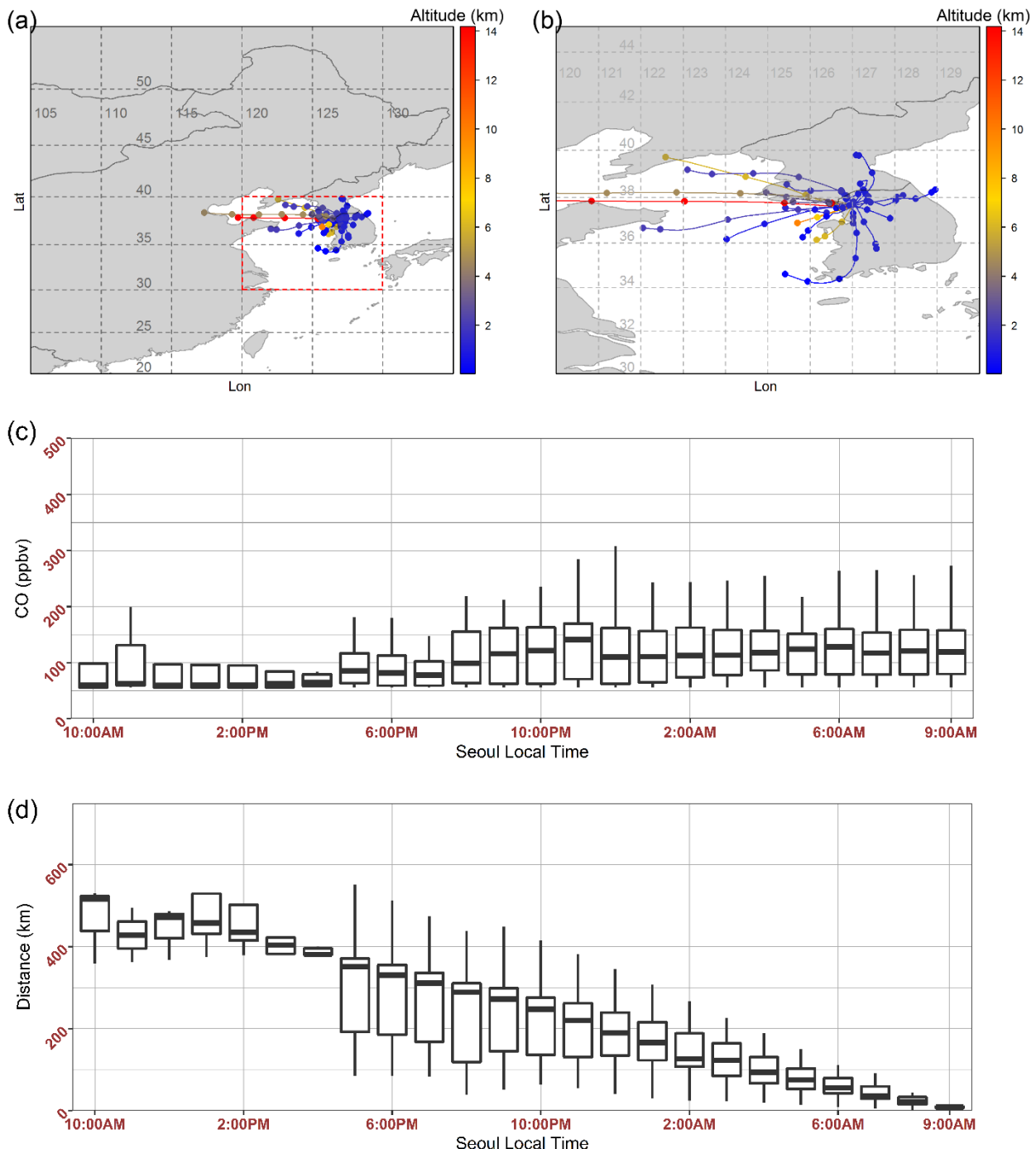
**Figure 6: C-TRAIL output for June 4, 2016: (a) the trajectory of packets reaching Seoul at 9:00 AM local time
(b) changes in the CO concentrations of four aged packets moving toward Seoul from source points**



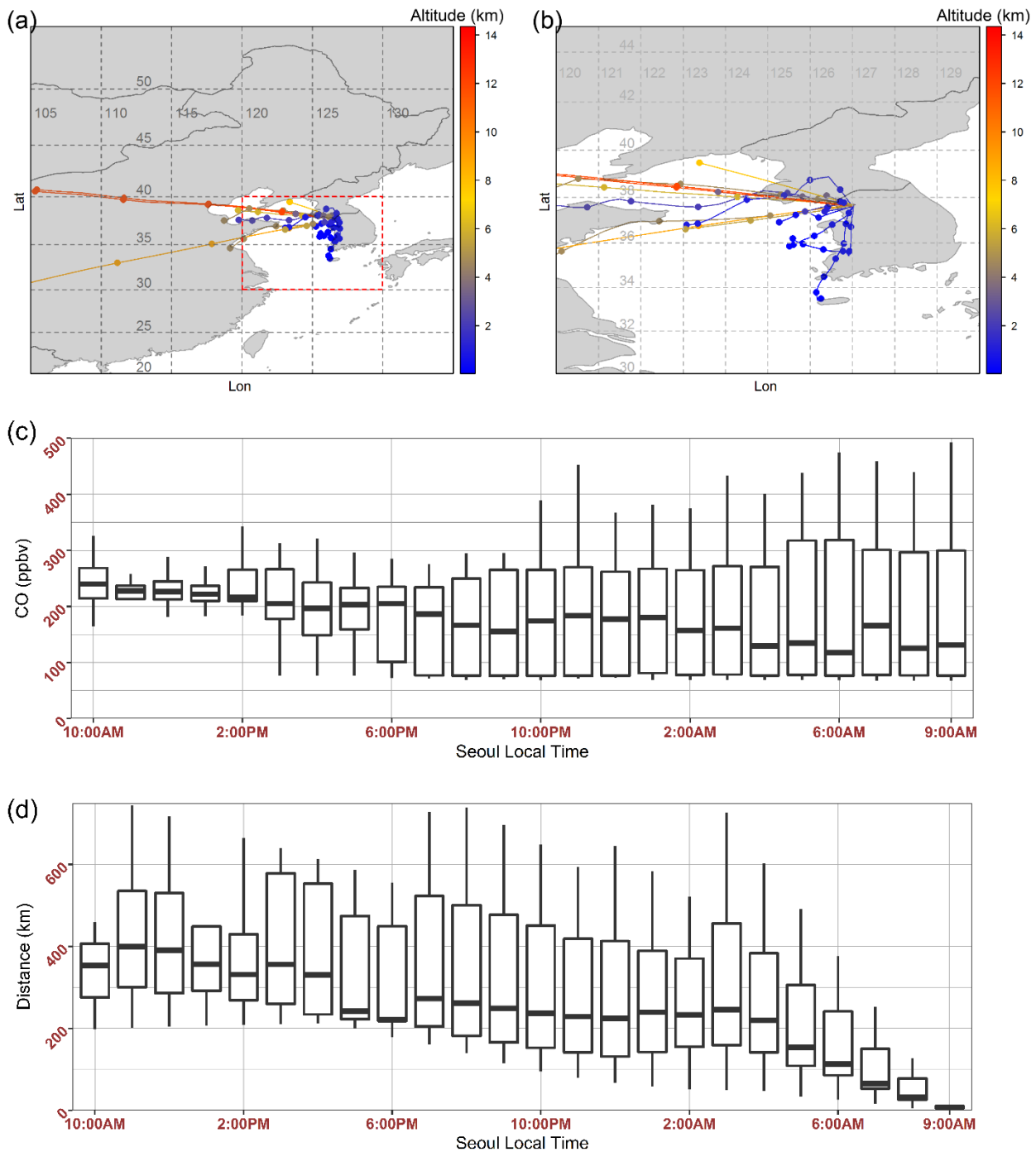
534
 535
 536
 537 **Figure 7: C-TRAIL output for the entire month of May 2016 for Seoul as the receptor: (a) 24-hour trajectories of packets for the**
entire domain, (b) 24-hour trajectories of packets for the zoomed area in South Korea, (c) the boxplot of the CO concentrations of
all packets at each hour before they reached Seoul, and (d) the boxplot of packet distances from Seoul every hour before the
packets reached Seoul



538
 539
 540
 541 **Figure 8: C-TRAIL output for the dynamic weather period (DWP) for Seoul as the receptor: (a) 24-hour trajectories of packets**
for the entire domain, (b) 24-hour trajectories of packets for the zoomed area in South Korea, (c) the boxplot of the CO
concentrations of all packets at each hour before they reached Seoul, and (d) the boxplot of packet distances from Seoul every
hour before the packets reached Seoul

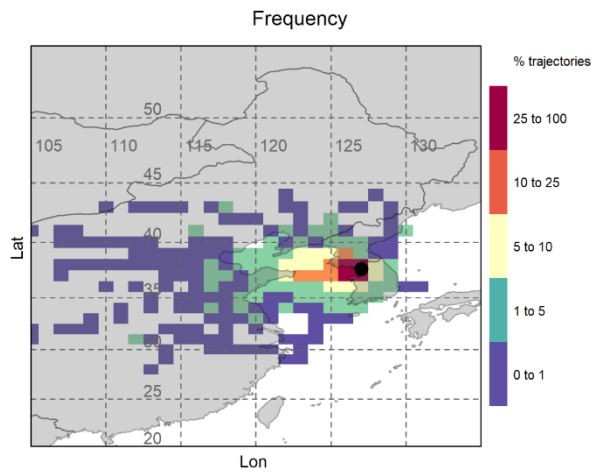


542
 543
 544
 545
 Figure 9: C-TRAIL output for the stagnant period (SP) for Seoul as the receptor: (a) 24-hour trajectories of packets for the entire
 546 domain, (b) 24-hour trajectories of packets for the zoomed area in South Korea, (c) the boxplot of the CO concentrations of all
 547 packets at each hour before they reached Seoul, and (d) the boxplot of packet distances from Seoul every hour before the packets
 548 reached Seoul



546
547
548
549 **Figure 10: C-TRAIL output for the extreme pollution period (EPP) for Seoul as the receptor: (a) 24-hour trajectories of packets**
for the entire domain, (b) 24-hour trajectories of packets for the zoomed area in South Korea, (c) the boxplot of the CO
concentrations of all packets at each hour before they reached Seoul, and (d) the boxplot of packet distances from Seoul every
hour before the packets reached Seoul

550 (a)



(b)

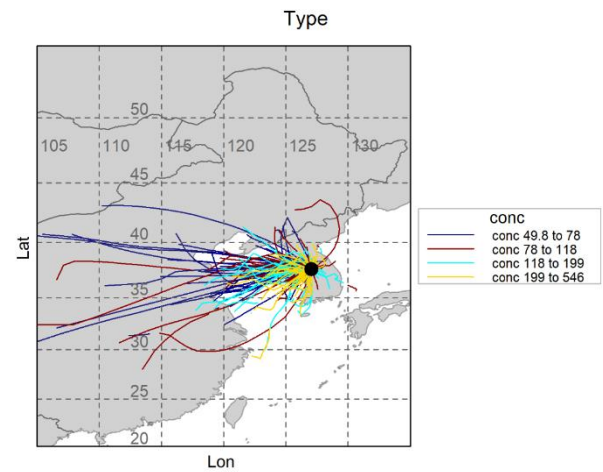
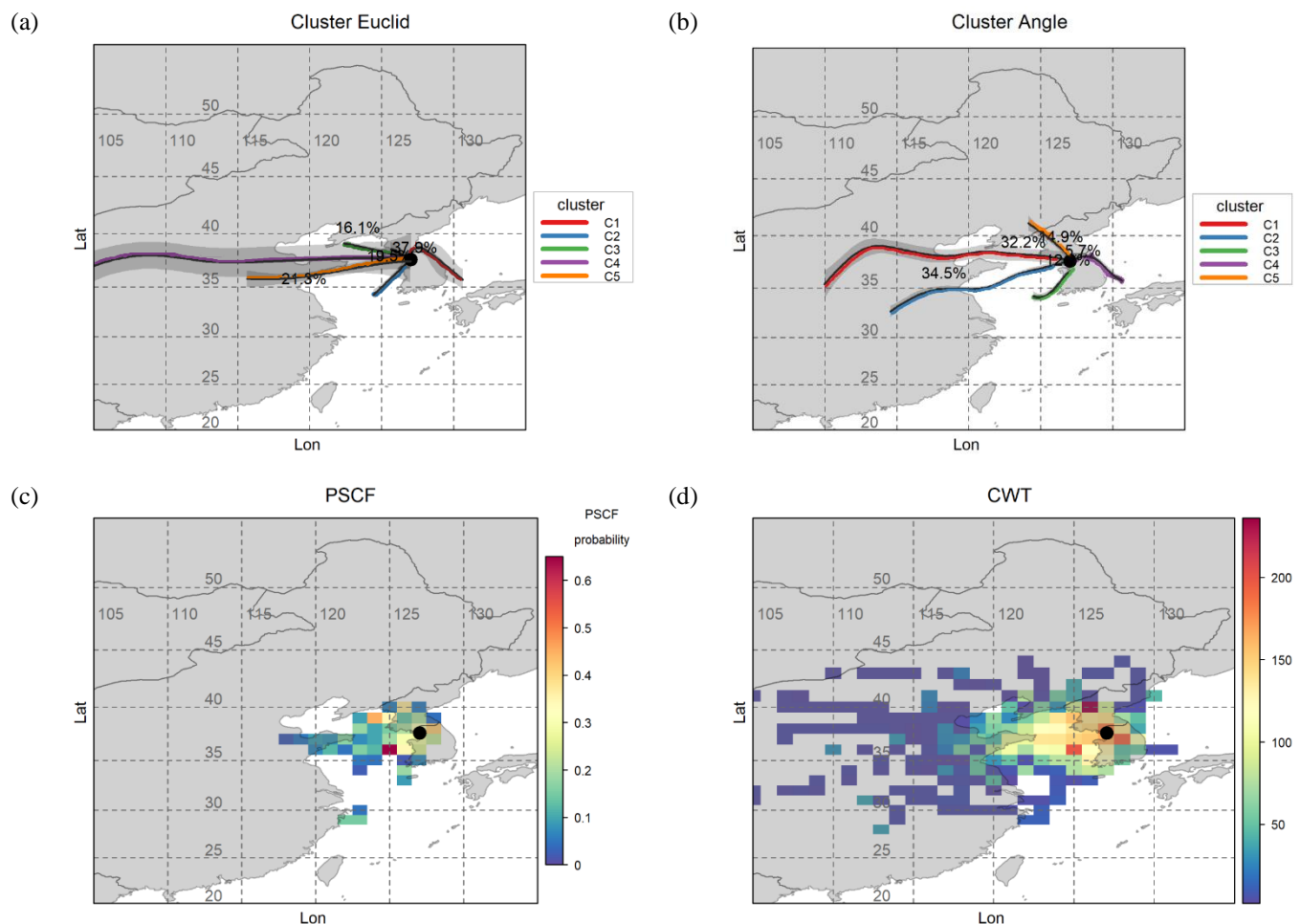


Figure 11: (a) Plot of the frequency of trajectories and (b) the trajectories, classified by their concentration values

551



553 **Figure 12: (a) Trajectories clustered by the Euclidian distance function, (b) trajectories clustered by the angle distance function,**
 554 **(c) the potential source contribution factor plot, and (d) the concentration-weighted trajectory plot**